https://doi.org/10.5194/essd-2025-232
Preprint. Discussion started: 16 June 2025

Open Access Earth System Science Data Discussions

Urban Eddy Covariance – The INFLUX Network

Jason P Horne[1], Scott J Richardson[1], Samantha L Murphy[1], Helen C Kenion[1], Bernd J Haupt[2], Benjamin J Ahlswede[1], Natasha L Miles[1], Kenneth J Davis[1, 2]
[1]Department of Meteorology and Atmospheric Science, The Pennsylvania State University, University Park, 16802, PA, USA
[2]Earth and Environmental Systems Institute, The Pennsylvania State University, University Park, 16802, PA, USA
Correspondence to: Kenneth J Davis (kjd10@psu.edu)

Abstract. The eddy covariance method is used by various disciplines to measure surface-atmosphere fluxes of both vector and scalar quantities. However, eddy covariance observations are uncommon in urban areas. One of the few long-term and ongoing urban flux experiments is the Indianapolis Flux Experiment (INFLUX), which has successfully deployed eddy covariance towers at eleven locations measuring fluxes from various land cover types in and around the urban environment. The data collected from this network of towers has been used to determine urban greenhouse gas emissions, assess transport model performance, and separate anthropogenic from biogenic sources. This paper describes the available data associated with the INFLUX eddy covariance network, provides details of data processing and quality control, and provides site attributes needed to interpret the data. For access to the various data products from the INFLUX eddy covariance work, please see the data availability section below.

Short summary. We present data from a network of towers in Indianapolis used to study how heat and gases move between the surface and atmosphere in a city. This rare, long-term urban experiment helps us understand things like carbon emissions from these urban areas. We explain what was measured, how we checked data quality, and why these observations help improve our overall understanding of the urban environment.

https://doi.org/10.5194/essd-2025-232
Preprint. Discussion started: 16 June 2025

1 Introduction

Eddy covariance (EC) is a method for quantifying the transfer (i.e., flux) of mass, energy, and momentum between the surface and the atmosphere. Using EC, investigators can monitor a system with minimal disturbance over long periods, making it an attractive method for various disciplines (e.g., ecologists, meteorologists, hydrologists) (Baldocchi et al., 2001). The foundation of the technique is to sample the spectrum of turbulent eddies and the associated scalar constituents to calculate the covariance of the vertical wind component and the variable of interest. This covariance can be used to quantify the turbulent surface flux of a variable (vector or scalar) in many conditions (e.g. Yi et al. 2000). This method typically uses fast response (≥10Hz) instruments to measure the three-dimensional wind and various atmospheric scalars (e.g., CO_2, H_2O, temperature). A comprehensive description of the EC method can be found in Aubinet et al. 2012 and Burba 2013 or many micrometeorological-focused texts (Foken, 2008; Lee et al., 2004).

Urban EC work often involves quantifying greenhouse gas (GHG) emissions. Urban areas are responsible for 67-72% of anthropogenic CO_2 emissions globally (Lwasa et al., 2023). Many cities have pledged to reduce GHG emissions in this era of anthropogenic climate change. The EC method can directly measure GHG fluxes within the tower's footprint. For example, Liu et al., (2012) investigated spatial and temporal variability of CO_2 fluxes in the Beijing megacity using the EC method and found weekly (e.g., traffic volume) and seasonal (e.g., domestic heating) patterns in CO_2 fluxes. Crawford and Christen (2015) were able to disaggregate observed CO_2 fluxes into biogenic and anthropogenic sources by modeling various sources/sinks within the turbulent source area (i.e., flux footprint) of a residential area in Vancouver, Canada. Pawlak and Fortuniak (2016) assessed the temporal variability of CH_4 fluxes in a populated area of Łódź, Poland, and found the city's annual emissions (17.6 g m^{-2} $year^{-1}$) were comparable to surrounding natural sources like wetlands (18 g m^{-2} $year^{-1}$). Menzer and McFadden (2017) used statistical partitioning of CO_2 fluxes over a suburban neighborhood outside Saint Paul, Minnesota, (US-KUO: KUOM tower) to separate biogenic from anthropogenic sources.

Mixed fluxes are not unique to urban flux measurements. Ecosystem flux measurements have endeavored for years to disaggregate, for example, respiration from photosynthesis and transpiration from evaporation. Biological and anthropogenic CO_2 fluxes have been disaggregated using both statistical partitioning methods, which model some carbon source or sink (Crawford and Christen 2015; Lee et al. 2021; Menzer and McFadden 2017), and tracer ratio methods (Ishidoya et al. 2020; Wu et al. 2022). In a similar vein, the Indianapolis Flux Experiment (INFLUX; Davis et al., 2017) primarily investigates greenhouse gas (GHG) emissions in and around Indianapolis. The EC method continues to increase in popularity and accessibility, increasing the number of EC towers (i.e., flux towers) in operation. Despite this expansion in the number of towers contributing data to global networks like FLUXNET (https://fluxnet.org/), most flux towers monitor rural vegetative communities. Urban environments are underrepresented (Pastorello et al., 2020).

A handful of projects have successfully measured fluxes using EC in the urban environment (Biraud et al., 2021; Kotthaus and Grimmond, 2014; Menzer and McFadden, 2017; Vogt et al., 2006; Wu et al., 2022), and collaborative intercity comparisons have and continue to utilize the increasing number of urban EC measurements (Lipson et al., 2022; Nicolini et al., 2022; Papale et al., 2020). For example, Nicolini et al.

https://doi.org/10.5194/essd-2025-232
Preprint. Discussion started: 16 June 2025

Earth System Science Data
Open Access Discussions

(2022) compared thirteen EC towers in eleven different European cities to assess the impacts of COVID-19 on CO_2 emissions. Through this work, they found a significant relationship between factors such as the lockdown stringency index and relative CO_2 flux change (i.e., before vs. during lockdown), showing the value of EC measurements in detecting long and short-term changes in CO_2 fluxes in real time. Other efforts, such as the Urban-PLUMBER project (https://urban-plumber.github.io/), have gathered urban EC measurements from twenty towers located all over the world, creating a dataset of urban EC measurements covering a spectrum of different climatic conditions and urban forms used in model evaluation (Lipson et al., 2022).

While having a single tower in a city is invaluable, a single flux tower cannot represent the heterogeneous mosaic across the entire city. Having multiple towers within and outside a single city allows for intra-city comparisons and assessment of the urban-rural interface. For example, Nicolini et al. (2022) were able to use paired towers within the same city (e.g., residential vs. non-residential) to infer qualitative information on the dominant CO_2 driver (e.g., vehicular, vegetation, etc.). Peters et al. (2011) showed the benefit of measuring turfgrass lawns using a short-stature (1.35 m) tower to help interpret ET measurements made on the KUOM tall tower (40 m) in Saint Paul, Minnesota.

The urban greenhouse gas test beds program of the National Institute of Standards and Technology (Semerjian and Whetstone, 2021) has endeavored to "improve emission measurement tools to better equip decision makers and mitigation managers with capabilities to chart progress in GHG emissions mitigation" (https://www.nist.gov/greenhouse-gas-measurements/urban-test-beds). The INFLUX project is the longest-running test bed in this program. Atmospheric inversions are the primary technological approach employed for urban GHG emissions estimates in the test bed program (Karion et al., 2023; Lauvaux et al., 2020; Yadav et al., 2023) given their ability to encompass emissions from the entirety of an urban area. These approaches struggle, however, to infer the spatial structure of emissions within a city (Lauvaux et al., 2020). Eddy covariance flux towers, long used to study fluxes at a spatial resolution more accessible to local-scale, process-based model evaluation, have been deployed in INFLUX to complement whole-city atmospheric inversions.

The INFLUX EC flux towers have measured CO_2, H_2O, energy, and momentum fluxes in and around Indianapolis. The network includes EC flux observations from eleven locations (Fig. 1), comprising over a decade and a half of observation site years (Table 1, Fig. 2). These tower locations range from agricultural sites in the croplands surrounding Indianapolis to towers in the cities' interior over turfgrass, suburban forests, residential areas, and heavily developed urban regions (Fig. 1). This multiplicity of flux sites was achieved by moving instrumentation from site to site as deemed necessary to sample the variability in fluxes in and around this urban landscape. A subset of the flux measurements (Table 1) has been co-located with mole fraction observations (Richardson et al., 2017) from the INFLUX urban GHG testbed monitoring network (Miles et al., 2017a).

This paper documents the urban EC measurements undertaken as part of the INFLUX project. We discuss methods for quality-controlling the INFLUX EC measurements and describe the groups of EC flux sites within the INFLUX project (i.e., agricultural, turfgrass, and tall towers). We present the data processing required to interpret the data within this urban network and document the availability of data products.

https://doi.org/10.5194/essd-2025-232
Preprint. Discussion started: 16 June 2025

Open Access Earth System Science Data Discussions

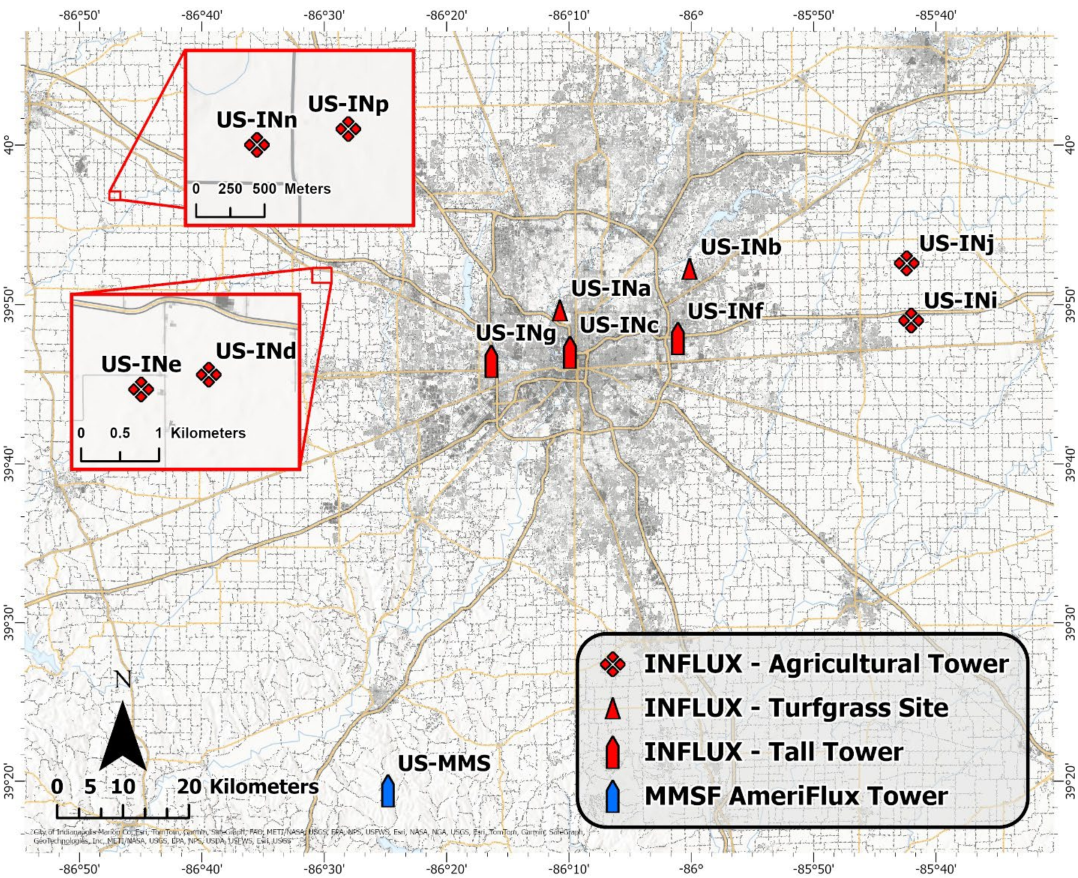

Figure 1. Locations of INFLUX eddy covariance towers in and around the city of Indianapolis. The gray shading represents the 2023 impervious surface cover from the National Land Cover Database (doi.org/10.5066/P9JZ7AO3). Major roadways are depicted using orange lines and waterways in light blue. The Morgan-Monroe State Forest (MMSF) AmeriFlux tower is also included for spatial reference. Service layer credits go to City of Indianapolis, Marion County, Esri, TomTom, Garmin, SafeGraph, FAO, METI/NASA, USGS, EPA, NPS, USFWS, and GeoTechnologies Inc.

2 INFLUX Eddy Covariance Tower Network

2.1 Flux tower sites and site categories

The INFLUX flux towers can be subdivided into heterogeneous (US-INc, US-INg, US-INf) and homogeneous sites. Within the homogenous grouping, we further subdivide the towers into agricultural (US-INd, US-INe, US-INi, US-INj, US-INn, US-INp) and turfgrass (US-INa, US-INb) categories. Each site is equipped with a sonic anemometer, either a Gill WindMaster (WindMaster, Gill Instruments, Lymington, UK) or CSAT3 (CSAT3, Campbell Scientific, Logan, UT, USA), and an infrared gas analyzer (LI-7500DS or LI-7500A LI-COR Biosciences, Lincoln, NE, USA) collecting data at 10Hz frequency (Table 2). The low-stature towers are also instrumented with a temperature and humidity probe (HMP155, Vaisala Oyj, Vantaa, Finland), and a subset are equipped with photosynthetically active radiation (PAR) sensors (LI190R, LI-COR Biosciences, Lincoln, NE, USA) (Table 2). US-INc and US-

https://doi.org/10.5194/essd-2025-232
Preprint. Discussion started: 16 June 2025

INg were equipped with 4-way net radiometers (CNR4, Kipp and Zonen, Delftechpark, Netherlands) in October 2023 and March 2024, respectively. In addition to the INFLUX EC towers, the AmeriFlux Core Site US-MMS (Figure 1), located in the Monroe-Morgan State Forest, is approximately seventy kilometers to the southwest of Indianapolis (Dragoni et al., 2011; Schmid et al., 2000).

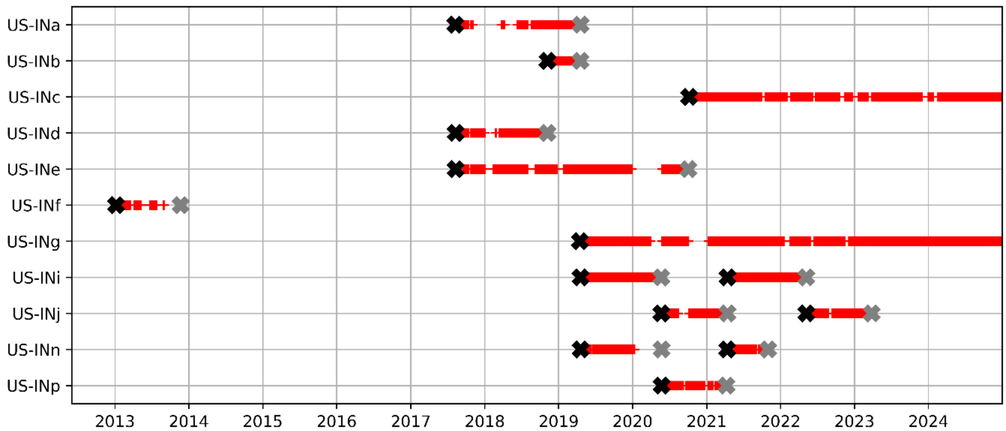

Figure 2: Data availability at each site through 2023. Each half-hour data point is indicated by a red "+", flux instrumentation deployment dates are indicated by black x's, and flux instrumentation decommissioning dates are indicated by gray x's. Any missing data between the deployment and decommissioning dates is due to power loss or instrument malfunction.

Table 1. Site identification in FLUXNET format, deployment period, and short description of each site.

Site	Time Start	Time End	Site Description
US-INa	August 2017	April 2019	Pioneer Cemetery in Crown Hill Cemetery tower measured a minimally managed turfgrass lawn.
US-INb	November 2018	April 2019	The Fort Golf Resort tower measured a heavily managed turfgrass lawn.
US-INc	October 2020	Current	Downtown Indianapolis tower measured an urbanized, heterogeneous area and is also mole fraction site 03*.
US-INd	August 2017	November 2018	An agricultural tower near Pittsboro measured a mixture of corn and soy.
US-INe	September 2017	October 2020	An agricultural tower near Pittsboro measured corn (2018 and 2020) and soy (2019).
US-INf	January 2013	November 2013	The tower at East 21st St measured a heterogeneous commercial and residential area and is also mole fraction site 02*.
US-INg	April 2019	Current	Wayne Twp Comm tower measures a heterogeneous residential and commercial area and is also mole fraction site 07*.

https://doi.org/10.5194/essd-2025-232
Preprint. Discussion started: 16 June 2025

US-INi	April 2019	May 2022	The agricultural tower measured soy (2019) and corn (2021). Located near mole fraction site 09[*].
US-INj	May 2020	March 2023	The agricultural tower measured corn during both growing seasons (2020 and 2022). Located near mole fraction site 09[*].
US-INn	April 2019	October 2021	Agricultural tower measured corn during 2019 and 2021. Located near mole fraction site 14[*].
US-INp	May 2020	April 2021	The agricultural tower measured a mixture of corn and turfgrass in 2020. Located near mole fraction site 14[*].

* Mole fraction towers and their numbers are described in Miles et al. (2017a).

Table 2. Measurement heights of deployed eddy covariance instruments and flux instruments for each site.

Site	EC measurement height	Infrared gas analyzer	Sonic anemometer	Temperature/ Humidity	PAR	Net Radiation	Arable
US-INa	3 m	Licor LI-7500A	Campbell CSAT3	Vaisala HMP155	-	-	-
US-INb	3 m	Licor LI-7500A	Campbell CSAT3	Vaisala HMP155	-	-	-
US-INc	43 m	Licor LI-7500A	Campbell CSAT3	-	-	Kipp & Zonen CNR4 (10/2023)	-
US-INd	3 m	Licor LI-7500A	Campbell CSAT3	Vaisala HMP155	-		-
US-INe	3 m	Licor LI-7500A	Campbell CSAT3	Vaisala HMP155	-		Yes
US-INf	30 m	Licor LI-7500A	Campbell CSAT3				-
US-INg	41 m	Licor LI-7500DS	Gill WindMaster	-	-	Kipp & Zonen CNR4 (03/2024)	-
US-INi	3 m	Licor LI-7500A	Campbell CSAT3	Vaisala HMP155	Licor LI190R	-	-
US-INj	3 m	Licor LI-7500A	Campbell CSAT3	Vaisala HMP155	Licor LI190R	-	Yes
US-INn	3 m	Licor LI-7500A	Campbell CSAT3	Vaisala HMP155	Licor LI190R	-	-

https://doi.org/10.5194/essd-2025-232
Preprint. Discussion started: 16 June 2025

US-INp	3 m	Licor LI-7500A	Campbell CSAT3	Vaisala HMP155	-	-	Yes

2.2 Data acquisition and organization

The INFLUX EC instruments produce 10 Hz GHG data files, each containing thirty minutes of continuous data; 48 files per day. The GHG file is then transferred from the logger to a Linux server using SFTP. Each instrument has a unique incoming directory where the files are stored. Every night, a set of shell scripts checks to see if all 48 files have been delivered. Furthermore, every night, GHG files are copied to an archive while the data files are checked for (i) readability for further processing (occasionally some files are corrupt), (ii) monotonically time increase of recorded data (will be automatically corrected if possible), (iii) any non-ASCII characters which could cause problems during further scientific processing), (iv) incomplete data rows. Emails are automatically generated if any fault is recognized, while copies of the automatically modified and corrected data files are saved. Each step is captured in a log file. Missing data, errors, and file modifications due to errors trigger an email notification. These checks test file integrity and completeness of data files. Once the integrity tests are completed, the data is automatically processed and analyzed using EddyPro (LI-COR, 2021) and Python scripts. Graphics of the processed data (two-week data window) are automatically updated online to manually monitor the incoming data and quickly identify and address issues. This lets researchers quickly see whether the instruments produce reasonable results or need immediate attention.

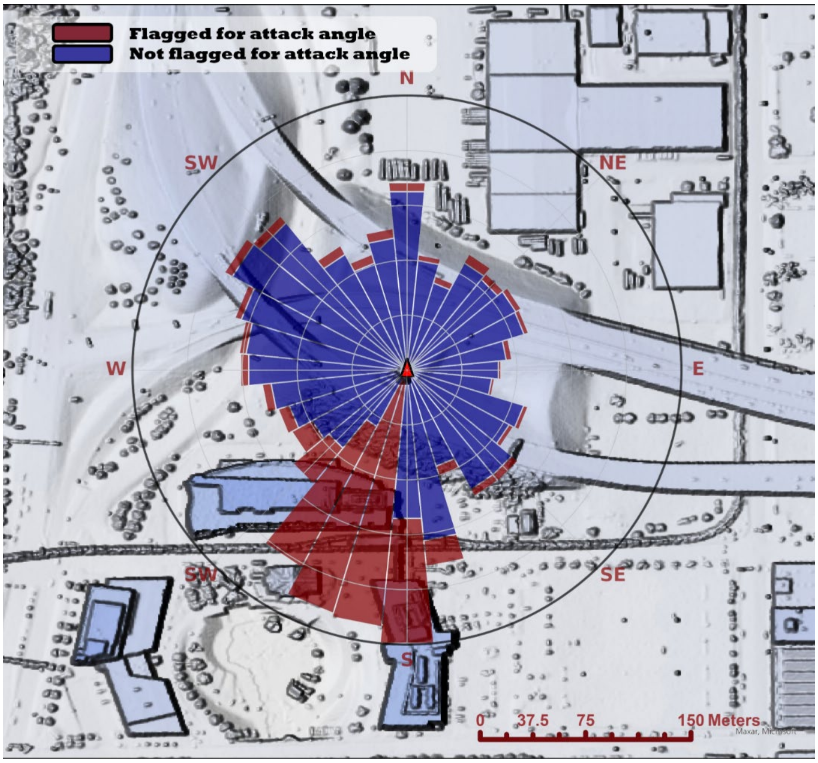

https://doi.org/10.5194/essd-2025-232
Preprint. Discussion started: 16 June 2025

Figure 3. Percent of total data (i.e., all wind directions) flagged (radial) as a binary attack angle flagging (red/blue) vs. wind direction (angular) at US-INc (Oct 2020 – Jan 2023). Radial scales show 1.1, 2.2, 3.3, 4.4, and 5.6 percent of the total data moving from the inner to the outer ring, respectively. The red triangle represents the location of US-INc. The base map is a digital surface map generated using 2016 Indiana Statewide 3DEP LiDAR Data Products for Marion County (USDA, 2016). Service layer credits go to Maxar and Microsoft.

2.3 Flux processing and quality control

The complete time series of fluxes are calculated separately from the automatic processing script using a set of distinct post-processing steps and the EddyPro software package. For a comparison between how EddyPro compares to other commonly used software (e.g., TK3 and eddy4R) when computing fluxes at tall urban flux towers, please see Lan et al. (2024). For every thirty minutes, we apply a block-averaging detrending (Foken, 2008; Lee et al., 2004) and planar fit coordinate rotation (Lee et al., 2004; Paw U et al., 2000; Wilczak et al., 2001). Only a planar fit rotation was applied to US-INf, and none of the following corrections or quality control tests were used. The Vickers and Mahrt (1997) despiking procedure is done before calculating fluxes, spikes are removed, and the number of spikes is reported. As the molar densities are measured by open-path sensors (LI-7500A or LI-7500DS), we apply the Webb, Pearman, and Leuning correction for density fluctuations (Lee and Massman, 2011; Paw U et al., 2000; Webb et al., 1980). The cospectra are corrected (high and lowpass) via the analytical methods of Moncrieff et al. (1997), which is based on the methods of Moore (1986) using the similarity-based cospectral models from Kaimal et al. (1972). For each averaging period, using the methods of Vickers and Mahrt (1997), a set of flags is generated based on the high-frequency measurements.

Flux data are flagged for violating an angle of attack test if >10% of the wind vectors exceed an attack angle of >|30º| for the averaging period. In the urban environment, the attack angle can be used to examine the impact of wake turbulence generated from roughness elements (RE) within the footprint of the tower. For example, wind directions from the southwest (180-225°) of US-INc (Fig. 3) are flagged ≥ 30% of the time, detecting wake turbulence generated by a 30m tall building 100m southwest of the tower. From these impacted wind directions, the fluxes measured are not within the inertial sublayer (i.e., constant flux layer) where traditional EC assumptions are potentially valid.

Fluxes are also flagged for violating one or more conditions under which the measured vertical covariance can directly relate to the surface flux. Stationarity tests are conducted for each half-hour using the methodology of Foken and Wichura (1996) and Vickers and Mahrt (1997). Modeled integral turbulence characteristics from flux variance similarity theory are compared to measured variances of winds and scalars using the methods of Foken and Wichura (1996). Depending on the degree of nonstationarity and deviation from flux similarity theory, as determined by the Foken and Wichura (1996) tests, each averaging period is assigned a value (1-9) based on the scheme of Mauder and Foken (2004). Given the heterogeneity level across the urban landscape, measurements from a tall urban tower likely seldom, if ever, meet the underlying assumptions of EC. Despite this, the measured covariance provides invaluable information regarding the turbulent exchange at the measurement height. Additionally, when comparing measurements made at these tall urban towers to similarity prediction, it should be noted that aerodynamic parameters like displacement height are often directionally dependent (Kent et al., 2018). Thus, the similarity-based relationship should scale differently depending on the wind direction. These

https://doi.org/10.5194/essd-2025-232
Preprint. Discussion started: 16 June 2025

subtle details are not included in the current version of EddyPro, but the software's default flags, generated (as discussed here), can still guide users in interpreting the data.

For two agricultural sites, US-INn and US-INp, periods of the high-frequency data were lost, and only a version of the processed thirty-minute data using the default EddyPro settings was recovered. At US-INn, the period is from 04-21-2019 00:00 UTC to 01-10-2020 03:30 UTC, and at US-INp, it is from 05-23-2020 21:30 UTC to 12-22-2020 16:00 UTC. For these periods, a double rotation rather than a planar fit is used, and fluxes are flagged based on a simplified version of the 1-9 scheme after the Spoleto agreement, 2004, for CarboEurope-IP, shown in Mauder Foken (2004). These periods of missing high-frequency data have been combined with those where the high-frequency data is available, meaning that there is a mixture of flagging scheme and coordinate rotation in some columns.

After calculating half-hourly fluxes, additional screening methods generate flags based on periods with weak gas analyzer signals, extreme flux values, or weak turbulence. The data are flagged if the signal strength reported by the gas analyzer for a half-hour period falls below the mean signal strength for a moving window of two weeks. Nighttime data (i.e., periods when the solar altitude is ≤ 0º) are flagged during low turbulent intensities based on the methods of Goulden et al. (1996). We acknowledge that the use of friction velocity filters in urban areas is still under question (Papale et al., 2022); a consensus has not been reached. We assert that this remains a valuable screening tool that we apply to this dataset. Finally, the flux data are flagged based on a threshold of N standard deviations from the mean, where N is a number specific to each site and is chosen to keep the variable magnitudes within geophysical limits.

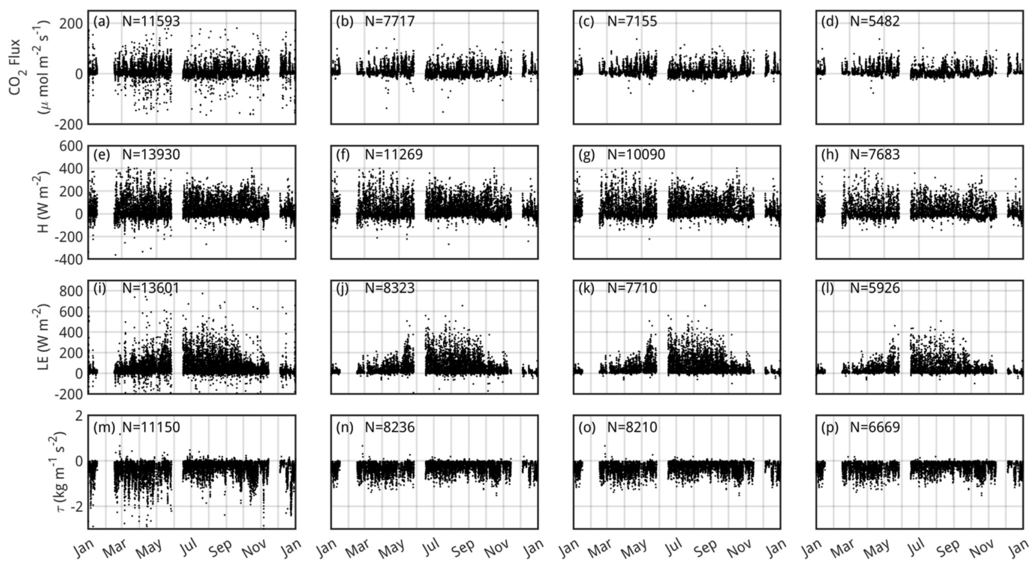

Figure 4. CO_2 fluxes (panels (a)-(d)), sensible heat fluxes (H) (panels (e)-(h)), latent heat fluxes (LE) (panels (i)-(l)), and momentum fluxes (τ) (panels (m)-(p)) at Site US-INg for 2022 with different quality control flags applied. From left to right, filtering sets 1, 2, 3, and 4, for each of the fluxes, are shown, representing a range of filtering choices from least to most strict. The number of points remaining in the dataset after removing quality control flags is indicated on each panel. With no filtering applied, there are

https://doi.org/10.5194/essd-2025-232
Preprint. Discussion started: 16 June 2025

Open Access Earth System Science Data Discussions

13,779 CO_2 flux data points, 13,969 sensible heat data points, 13,697 latent heat flux data points, and 13,969 momentum flux data points.

Table 3: Description of quality control flag combinations considered for CO_2, sensible heat (H), latent heat (LE), and momentum (τ) fluxes. Hard flag is abbreviated to hf in the table.

Flux	Set 1	Set 2	Set 3	Set 4
CO_2	Friction velocity CO_2 flux standard deviation	Friction velocity CO_2 flux standard deviation Spike hf w Amplitude resolution hf w Drop out hf w Absolute limits hf w Discontinuities hf w Spike hf CO_2 Amplitude resolution hf CO_2 Drop out hf CO_2 Absolute limits hf CO_2 Discontinuities hf CO_2 Signal strength	Friction velocity CO_2 flux standard deviation Spike hf w Amplitude resolution hf w Drop out hf w Absolute limits hf w Discontinuities hf w Spike hf CO_2 Amplitude resolution hf CO_2 Drop out hf CO_2 Absolute limits hf CO_2 Discontinuities hf CO_2 Signal strength CO_2 QC greater than 5	Friction velocity CO_2 flux standard deviation Spike hf w Amplitude resolution hf w Drop out hf w Absolute limits hf w Skewness and kurtosis hf w Discontinuities hf w Spike hf CO_2 Amplitude resolution hf CO_2 Drop out hf CO_2 Absolute limits hf CO_2 Discontinuities hf CO_2 Signal strength CO_2 QC greater than 5 Attack angle hf Nonsteady wind hf
H	H standard deviation	H standard deviation Spike hf w Amplitude resolution hf w Drop out hf w Absolute limits hf w Discontinuities hf w	H standard deviation Spike hf w Amplitude resolution hf w Drop out hf w Absolute limits hf w Discontinuities hf w H QC greater than 5	H standard deviation Spike hf w Amplitude resolution hf w Drop out hf w Absolute limits hf w Skewness and kurtosis hf w Discontinuities hf w H QC greater than 5 Attack angle hf Nonsteady wind hf
LE	H_2O flux standard deviation	H_2O flux standard deviation Spike hf w Amplitude resolution hf w	H_2O flux standard deviation Spike hf w Amplitude resolution hf w	H_2O flux standard deviation Spike hf w Amplitude resolution hf w

https://doi.org/10.5194/essd-2025-232
Preprint. Discussion started: 16 June 2025

		Drop out hf w Absolute limits hf w Discontinuities hf w Spike hf H_2O Amplitude resolution hf H_2O Drop out hf H_2O Absolute limits hf H_2O Skewness and kurtosis hf H_2O Signal strength	Drop out hf w Absolute limits hf w Discontinuities hf w Spike hf H_2O Amplitude resolution hf H_2O Drop out hf H_2O Absolute limits hf H_2O Skewness and kurtosis hf H_2O Signal strength LE QC greater than 5	Drop out hf w Absolute limits hf w Skewness and kurtosis hf w Discontinuities hf w Spike hf H_2O Amplitude resolution hf H_2O Drop out hf H_2O Absolute limits hf H_2O Skewness and kurtosis hf H_2O Signal strength LE QC greater than 5 Attack angle hf Nonsteady wind hf
τ	Wind directions impacted by tower distortion	Wind directions impacted by tower distortion Spike hf w Amplitude resolution hf w Drop out hf w Absolute limits hf w Discontinuities hf w Spike hf v Amplitude resolution hf v Drop out hf v Absolute limits hf v Discontinuities hf v Spike hf u Amplitude resolution hf u Drop out hf u Absolute limits hf u Discontinuities hf u Attack angle hf	Wind directions impacted by tower distortion Spike hf w Amplitude resolution hf w Drop out hf w Absolute limits hf w Discontinuities hf w Spike hf v Amplitude resolution hf v Drop out hf v Absolute limits hf v Discontinuities hf v Spike hf u Amplitude resolution hf u Drop out hf u Absolute limits hf u Discontinuities hf u QC τ greater than 5 Attack angle hf	Wind directions impacted by tower distortion Spike hf w Amplitude resolution hf w Drop out hf w Absolute limits hf w Skewness and kurtosis hf w Discontinuities hf w Spike hf v Amplitude resolution hf v Drop out hf v Absolute limits hf v Skewness and kurtosis hf v Discontinuities hf v Spike hf u Amplitude resolution hf u Drop out hf u Absolute limits hf u Skewness and kurtosis hf u Discontinuities hf u QC τ greater than 5

https://doi.org/10.5194/essd-2025-232
Preprint. Discussion started: 16 June 2025

	Attack angle hf
	Nonsteady wind hf

We provide processed, half-hourly flux datasets for each of the eleven INFLUX sites through Penn State Data Commons and Ameriflux (See Section 3). We do not remove data based on the generated flag for the data set available on Penn State Data Commons; instead, we leave the filtering decisions to the user. For most use-cases, we do not recommend eliminating all points flagged using the quality control flags provided using the methods Vickers and Mahrt (1997) and Mauder and Foken (2004) because of the large proportion of physically reasonable data flagged. We give an example of four different quality control flag combinations for CO_2, latent heat, sensible heat, and momentum fluxes using observations at Site US-INg in Fig. 4. The four quality control flag combinations for each of these fluxes are summarized in Table 3. We recommended at minimum filtering the data according to friction velocity and CO_2 flux standard deviation flags for analysis of CO_2 fluxes, sensible heat standard deviations flags for analysis of sensible heat fluxes, latent heat standard deviation flags for analysis of latent heat fluxes, and removing wind directions from which the measurement is impact by distortion due to the tower (for Site US-INg, observations from wind directions 30-135 should be removed) for momentum fluxes (Set 1 in Table 3). To remove additional outlier points, we suggest filtering by Sets 2 and 3 (Table 3) as shown in Fig. 4b and Fig. 4c for CO_2 fluxes, Fig. 4f and Fig. 4g for sensible heat fluxes, Fig. 4j and Fig. 4k for latent heat fluxes, and Fig. 4n and Fig. 4o for momentum fluxes. Given the significant reduction of overall data points, we do not suggest the flagging combination of Set 4, as shown in Fig. 4d, h, l, and p, unless the application of the data requires the strictest turbulence screening, which is appropriate only if the most idealized conditions for EC flux measurements are needed. At the tall urban flux towers (US-INc and US-INg), we recommend not removing CO_2 flux data based on the Vickers and Mahrt (1997) higher-moment statistics (i.e., skewness and kurtosis) since at these sites, these flags commonly target realistic data (Järvi et al., 2018). This is due to the urban environment's spatial and temporal source heterogeneity, which can cause the distribution of the high-frequency CO_2 measurement for a single period to often exceed the default skewness or kurtosis thresholds in EddyPro.

https://doi.org/10.5194/essd-2025-232
Preprint. Discussion started: 16 June 2025

Open Access Earth System Science Data Discussions

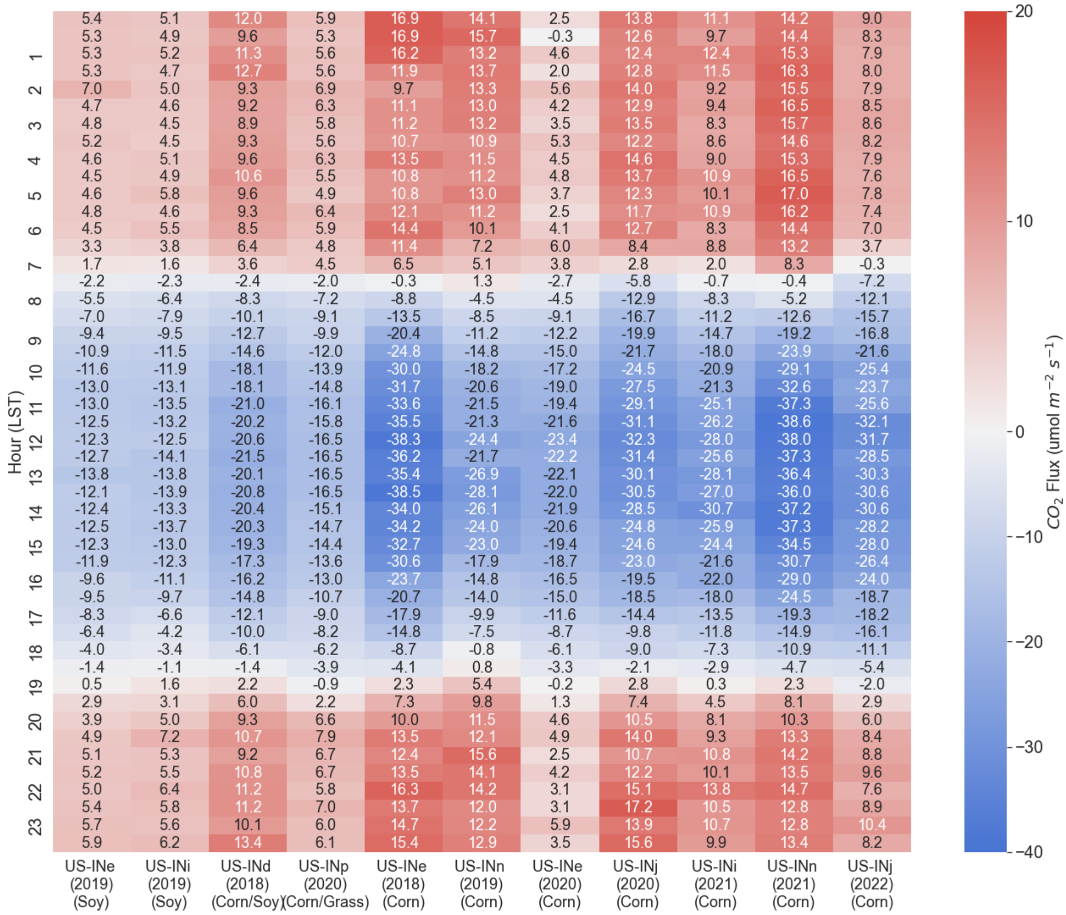

Figure 5. The average summer (JJA) diel cycle of CO_2 fluxes for each agriculture site-year. Each column is also labeled with the surrounding vegetation. The numbers indicate the average value for each half-hour flux corresponding to the underlying color. Text color is for visual purposes only.

2.4 Agricultural Sites

Understanding the boundary layer dynamics and CO_2 fluxes surrounding a city is important for understanding measurements collected within the city. The area surrounding Indianapolis is mainly composed of agricultural fields planted with a rotation of corn and soybeans. We deployed short-stature (~3-m AGL) flux towers at six locations in agricultural fields within 30-60 km of downtown Indianapolis (Fig. 1). The instrumentation for the agricultural sites (US-INd, US-INe, US-INn, US-INp) was, in most cases, relocated annually to sample a variety of fields. Each location was given a different site key. To supplement the flux measurements, soil cores were collected from US-INp, US-INn, US-INi, and US-INe and analyzed for percent nitrogen, carbon, pH, and concentrations of nutrients and trace elements (K, Mg, Ca, Zn, Cu, S). Additionally, Arable (Arable Mark 2, Arable, San Francisco, CA, USA) sensors were deployed at agricultural sites (US-INi, US-INj, US-INn, US-INp) beginning in 2020 to collect biometeorological measurements (e.g., NDVI, VPD, incoming solar radiation). We collected data at the six agricultural sites for eleven growing seasons (Fig. 5).

Flux footprint analyses are used to identify averaging periods when these agricultural towers may have been strongly influenced by vegetation other than the crops to be sampled. These conditions arise because of the practical need to place the flux towers close to but not directly within the actively managed crop fields. The fractional coverage of the agricultural crop of interest (corn or soybean) within the estimated tower footprint was calculated for each agricultural flux site in the INFLUX network. The calculated fractional coverage values allow a data user to select thresholds for which they would consider the half-hourly flux value representative of the vegetation of interest. The Flux Footprint Prediction (FFP) model by Kljun et al. (2015) is used to produce the vegetation fraction for each point in the data record. Imagery from Google Earth and ArcGIS Pro software is used to visually select areas covered with the vegetation of interest. Areas with the vegetation type of interest are assigned a value of one, while other areas are assigned a value of zero. For all half hours during which the required input data are available, the FFP climatology function simulates footprints at a 1 m grid spacing for a 501 m by 501 m domain. The site map distinguishing landcover types and the footprint estimate is multiplied to obtain a gridded map representing only the footprint attributable to the vegetation of interest. For every possible half hour, two values are computed using the predicted footprints: a value representing the footprint attributable to the vegetation of interest and a value for the total footprint. The former is calculated by summing over the footprint attributable to the vegetation of interest, and the latter by summing the footprint over the entire domain. The ratio of these values represents the fraction of the footprint attributable to the vegetation of interest.

2.5 Turfgrass Sites

Turfgrass is a common urban land cover (Milesi et al., 2005). Only a handful of towers have previously been deployed to measure turfgrass lawns (i.e., mixed species low-stature vegetation often artificially managed through irrigation, fertilization, and/or mowing) (Ng et al., 2015; Pahari et al., 2018; Pérez-Ruiz et al., 2020; Peters and McFadden, 2012) despite these lawns being an abundant vegetative community in urban areas (Horne et al., 2025). We deployed two flux towers (US-INa and US-INb) to monitor turfgrass lawns. The two INFLUX turfgrass towers captured different levels of management intensity. US-INa measured fluxes over a cemetery lawn (Fig. 6) with lower intensity management (i.e., infrequent mowing, no fertilization, and no irrigation), and US-INb measured fluxes over a golf course (i.e., frequent mowing, fertilization, and irrigation). These towers were of low stature and sited to minimize contributions to the flux footprint from anything other than turfgrass. We have used the CO_2 flux data from these two turfgrass towers to evaluate the Vegetation Photosynthesis and Respiration Model (VPRM) performance at reproducing seasonal turfgrass fluxes, finding that these lawns require a unique representation in the VPRM (Horne et al., 2025).

https://doi.org/10.5194/essd-2025-232
Preprint. Discussion started: 16 June 2025

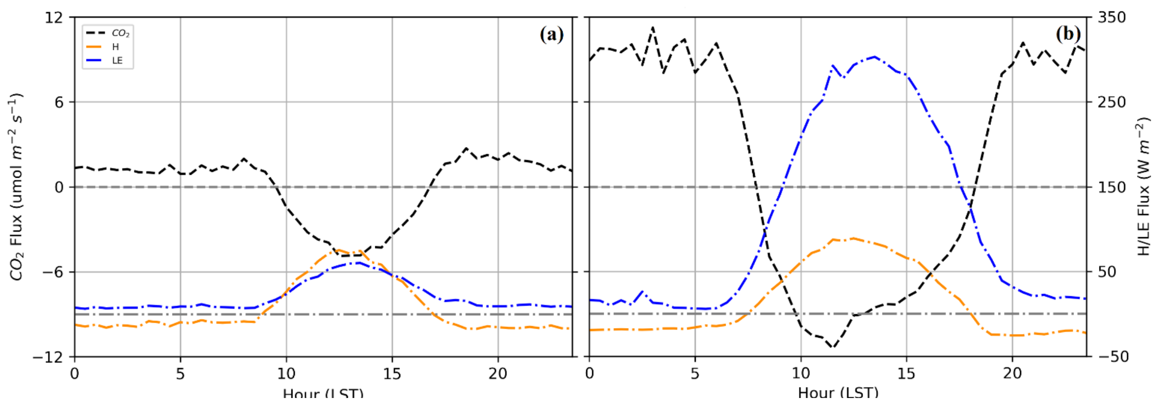

Figure 6. The average winter (DJF) (a) and summer (JJA) (b) diel cycle of latent heat (LE), sensible heat (H), and CO_2 fluxes for US-INa (cemetery lawn). Data for averaging are taken from the periods over the site deployment (Aug 2017 – April 2019).

2.6 Heterogeneous Footprint (Mixed) Urban Flux Towers

Three communications towers with EC instrumentation at 30 to 43 m AGL were instrumented to measure fluxes from the complex, mixed land cover typical of urban environments. These higher altitude measurements are necessary to measure fluxes above the trees and buildings commonly found across the metropolitan area. As mentioned, these towers host flux instrumentation and mole fraction measurements that are part of the INFLUX urban GHG testbed monitoring network (Miles et al., 2017a; Davis et al., 2017). Footprint climatologies for the INFLUX mixed urban flux towers are shown in Figs. 7 - 9. We include footprint climatologies for these sites alone to show the level of heterogeneity at each site and the estimated area measured by these towers. These footprint climatologies guide our characterization of the regions sampled by these towers. We describe broad characteristics of the urban landscapes in their flux footprints following the example of the Urban-PLUMBER project (https://urban-plumber.github.io/, Lipson et al., 2022). Table 4 provides metadata for the area surrounding the three heterogeneous urban flux towers (US-INc, US-INf, US-INg).

Table 4. Metadata for the surrounding land cover at the three tall flux towers. The domain is 4 km^2 centered around the respective tower and separated into quadrants NE [0-90°), SE [90-180°), SW [180-270°), and NW [270-360°) to capture heterogeneity surrounding the tower. Data for percent impervious and canopy fractions come from the National Land Cover Database (NLCD) using data for 2021 (US-INc and US-INg) and 2013 (US-INf) (doi.org/10.5066/P9JZ7AO3). LiDAR data used to estimate roughness elements (RE) (buildings and trees ≥2m) characteristics comes from the 2016 Indiana Statewide 3DEP LiDAR Data Products for Marion County (USDA, 2016). Roughness element density is the ratio of surface area occupied by REs to total surface area (i.e., planar area index).

Site	Quadrant	LCZ	Percent impervious (%)	Percent tree canopy	RE density	Mean RE height (m)	RE standard deviation (m)	Maximum RE height (m)

https://doi.org/10.5194/essd-2025-232
Preprint. Discussion started: 16 June 2025

				cover (%)				
US-INc (43m AGL)	NE	LCZ 8 (Large low-rise)	86	1	0.29	10.6	8.9	53
	SE	LCZ 8 (Large low-rise)	85	2	0.32	9.4	8.7	57
	SW	LCZ 6 (Open low-rise)	69	5	0.33	6.9	5.2	36
	NW	LCZ 6 (Open low-rise)	58	6	0.23	5.8	3.7	25
US-INf (30m AGL)	NE	LCZ 8_{Bc} (Large low-rise with scattered trees)	67	4	0.27	6.1	2.7	30
	SE	LCZ 6 (Open low-rise)	41	12	0.31	5.1	2.4	25
	SW	LCZ 6 (Open low-rise)	41	14	0.43	5.2	2.4	31
	NW	LCZ 6 (Open low-rise)	49	11	0.35	5	2.1	23
US-INg (41m AGL)	NE	LCZ 8_B (Large low-rise with scattered trees)	64	4	0.19	5.4	2.1	25
	SE	LCZ 6 (Open low-rise)	50	6	0.22	5.4	2.2	22
	SW	LCZ 6 (Open low-rise)	35	12	0.33	5.4	2.6	34
	NW	LCZ 6 (Open low-rise)	42	15	0.33	4.9	2.2	22

A complication with EC measurements of atmospheric constituents in urban areas is that urban systems are influenced by both anthropogenic and biogenic components. Wu et al. (2022) demonstrated a method of disaggregation using INFLUX EC data and the mole fraction measurement profiles available at the three INFLUX mixed urban flux towers (Richardson et al., 2017; Miles et al., 2017a) and tracer ratio methods. This methodology estimates the fossil fuel component of the CO_2 flux using carbon monoxide (CO) flux estimates combined with measurements of the CO to CO_2 flux ratio from fossil fuel combustion (Turnbull et al., 2015). The biogenic CO_2 flux is then determined by subtracting the fossil fuel flux from the total CO_2 flux measured via EC. Wu et al. (2022) demonstrated the promise of this technique via comparisons to the Hestia urban emissions inventory. Vogel et al. (2024) applied this methodology to study changes in emissions caused by the COVID-19 lockdown.

https://doi.org/10.5194/essd-2025-232
Preprint. Discussion started: 16 June 2025

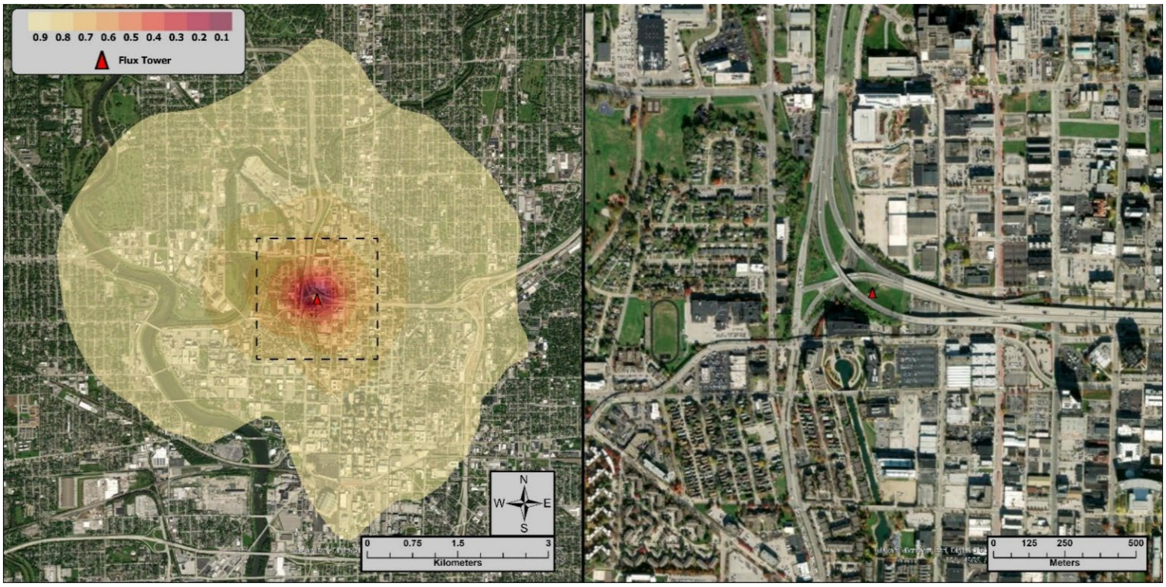

Figure 7. The left image shows a footprint climatology over a satellite image (2022) for US-INc (43m AGL), produced using all data from 2022, and the Kljun et al. (2015) flux footprint prediction (FFP) model. The outermost footprint boundary represents 90% of the footprint area. Wind directions impacted by the building wake (Fig. 2) are removed. The right image shows a zoomed-in image of a satellite image from 2022, whose boundary is marked by the dashed line on the left figure. Service layer credits go to Maxar, Microsoft, Esri, DigitalGlobe, FSA, USGS, and Earthstar.

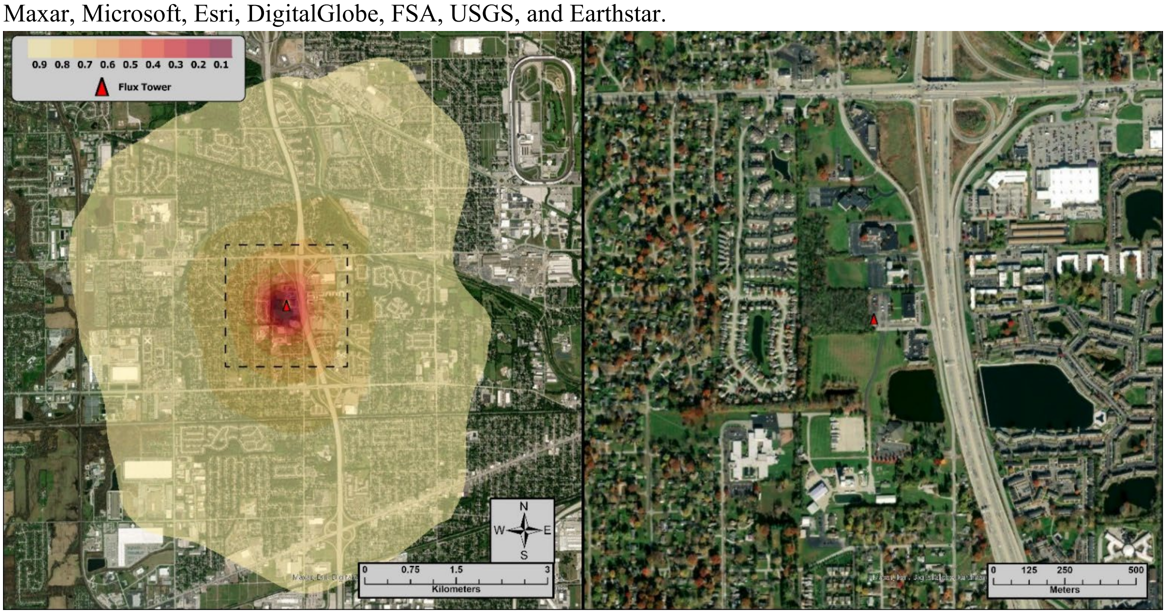

Figure 8. The left image shows a footprint climatology over a satellite image (2022) for US-INg (41m AGL), produced using all data from the 2022 annual year, and the Kljun et al. (2015) flux footprint prediction (FFP) model. The outermost footprint boundary represents 90% of the footprint area. The right

https://doi.org/10.5194/essd-2025-232
Preprint. Discussion started: 16 June 2025

Open Access Earth System Science Data Discussions

image shows a zoomed-in image of a satellite image from 2022, whose boundary is marked by the dashed line on the left figure. Service layer credits go to Maxar, Microsoft, Esri, DigitalGlobe, FSA, USGS, and Earthstar.

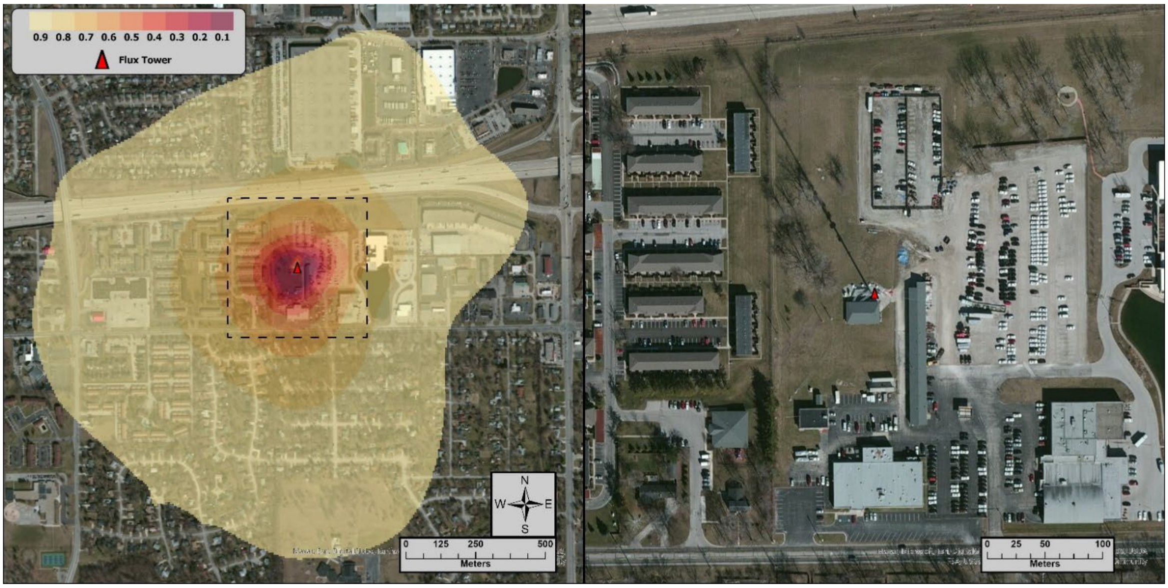

Figure 9. The left image shows a footprint climatology over a satellite image (2013) for US-INf (30m AGL), produced using all data available for US-INf, and the Kljun et al. (2015) flux footprint prediction (FFP) model. The outermost footprint boundary represents 90% of the footprint area. The right image shows a zoomed-in image of a satellite image from 2013, whose boundary is marked by the dashed line on the left figure. Service layer credits go to Maxar, Microsoft, Esri, DigitalGlobe, FSA, USGS, and Earthstar.

Two mixed urban flux towers, US-INf and US-INg, can each be interpreted as two distinct flux tower sites. We describe these differences in terms of building and vegetation cover (Table 4) and local climate zones (LCZ) (Stewart and Oke, 2012). The EC instruments at US-INg, for example, are set between a highway (LCZ E – Bare rock or paved) and commercial buildings (LCZ 8_B – Large low-rise with scattered trees) to the east and a forested residential neighborhood (LCZ 6 - Open low-rise) to the west. The two sectors exhibit dissimilar diel patterns of CO_2 fluxes (Fig. 10). To the west, we observe a photosynthetic drawdown from the suburban forest during the growing season. To the east, we can see two distinct peaks in net emissions corresponding to morning and evening rush hour traffic (Vogel et al., 2024). We suggest interpreting these data independently, essentially as two distinct flux towers, each of which senses a somewhat homogeneous (though mixed source) flux footprint. Similarly, the footprint at US-INf is divided roughly into northerly and southerly sectors (Table 4), with highway and commercial areas to the north and residences to the south.

https://doi.org/10.5194/essd-2025-232
Preprint. Discussion started: 16 June 2025

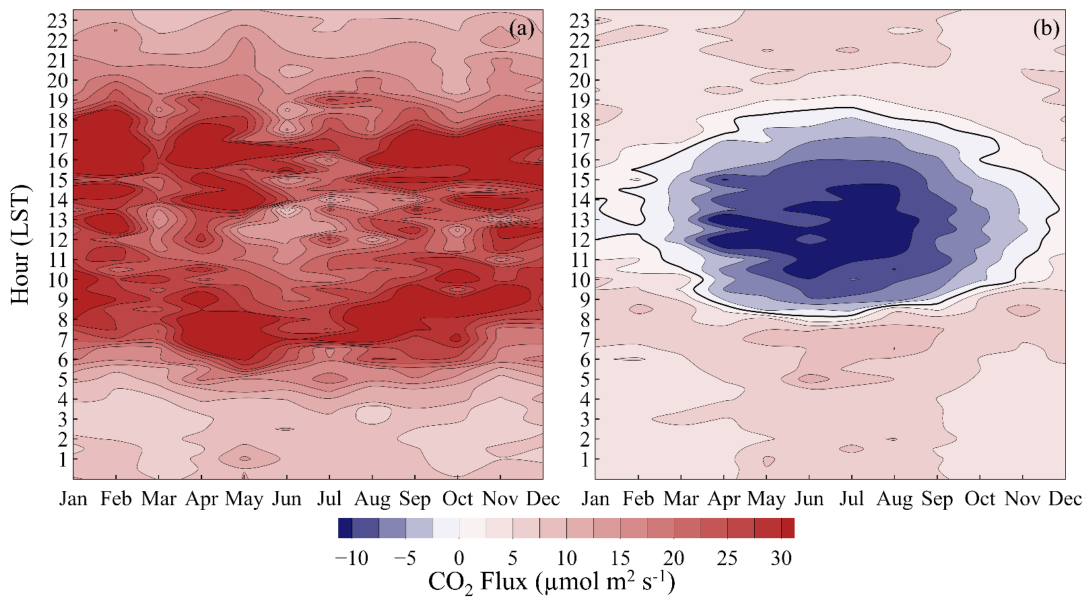

Figure 10. Isopleths of measured CO_2 flux at US-INg (April 2019 - January 2023) as a function of time of year (x-axis) and time of day (y-axis) for a) westerly wind directions (180 - 360º] and b) easterly wind directions (0 - 180º]. Positive values indicate net emissions of CO_2; negative values indicate a net uptake of CO_2.

We have not divided the flux data from US-INf and US-INg into two distinct records, nor have we posted flux footprint data sets to accompany each flux tower. However, the flux tower records contain all the data needed to subdivide the data sets and produce flux footprints. We note that urban systems frequently violate the assumptions implicit in current flux footprint models (e.g., homogeneous turbulence forcing in the flux footprint). We argue that existing footprint models (e.g., Kljun et al., 2015) are still quite helpful in interpreting these data sets, but that more research into the sensitivity of these models to complex urban systems is warranted.

3 Data availability

Unprocessed 10Hz data and processed INFLUX data are available on Penn State Data Commons (Table 5). This version contains all the processed data with flagging, but no data has been removed based on flagging. This processed data also included a metadata file describing the naming convention of variables and flagging. Data from all agriculture sites includes calculated fractional coverage and ancillary biometeorological data collected using the Arable sensors on site.

Table 5. Citations for each INFLUX tower. The raw data collected directly from the instruments, a processed version of the data available on Ameriflux, and a processed version with no flagged data removed are available through Penn State Data Commons.

Site	10Hz Data/full processed dataset	Ameriflux

https://doi.org/10.5194/essd-2025-232
Preprint. Discussion started: 16 June 2025

US-INa	Richardson et al. (2023a) - https://doi.org/10.26208/CJTC-KS26	Davis (2023a) - https://doi.org/10.17190/AMF/2001300
US-INb	Richardson et al. (2023a) - https://doi.org/10.26208/CJTC-KS26	Davis (2023b) - https://doi.org/10.17190/AMF/2001301
US-INc	Richardson et al. (2023b) - https://doi.org/10.26208/fsy8-h855	Davis (2023c) - https://doi.org/10.17190/AMF/1987603
US-INd	Richardson et al. (2023c) - https://doi.org/10.26208/2NT2-RS82	Davis (2023d) - https://doi.org/10.17190/AMF/2001302
US-INe	Richardson et al. (2023c) - https://doi.org/10.26208/2NT2-RS82	Davis (2023e) - https://doi.org/10.17190/AMF/2001303
US-INf	Sarmiento and Davis (2017) - https://doi.org/10.17190/AMF/2001304	Davis (2023f) - https://doi.org/10.17190/AMF/2001304
US-INg	Richardson et al. (2023b) - https://doi.org/10.26208/fsy8-h855	Davis (2023g) - https://doi.org/10.17190/AMF/2001305
US-INi	Richardson et al. (2023c) - https://doi.org/10.26208/2NT2-RS82	Davis (2023h) - https://doi.org/10.17190/AMF/2001306
US-INj	Richardson et al. (2023c) - https://doi.org/10.26208/2NT2-RS82	Davis (2023i) - https://doi.org/10.17190/AMF/2001307
US-INn	Richardson et al. (2023c) - https://doi.org/10.26208/2NT2-RS82	Davis (2023j) - https://doi.org/10.17190/AMF/2001308
US-INp	Richardson et al. (2023c) - https://doi.org/10.26208/2NT2-RS82	Davis (2023k) - https://doi.org/10.17190/AMF/2001309

In addition, all INFLUX EC datasets are available through the Ameriflux network (https://ameriflux.lbl.gov/, Table 5). As of May 2025, two of the eleven INFLUX flux locations (US-INc and US-INg) are actively collecting data. Data collected from active sites will be processed, updated, and made available through the Ameriflux network annually.

These flux measurements are a component of a broader research effort, the Indianapolis Flux Experiment (INFLUX). Multiple additional measurements and model data sets exist, creating a more complete experimental data set to assess urban greenhouse gases in Indianapolis, IN. These include mole fraction measurements (Miles et al., 2017b), flask measurements (https://gml.noaa.gov/dv/site/?stacode=INX), Doppler lidar measurements (https://csl.noaa.gov/projects/influx/), anthropogenic inventories (Gurney et al., 2018), and aircraft measurements (https://influx.psu.edu/influx/data/flight/), Vegetation Photosynthesis and Respiration Model (VPRM) simulations (Horne and Davis, 2024; Murphy et al., 2024), and Weather Research and Forecast (WRF) Reanalysis (Deng et al., 2020), which are not described in detail here. For more information concerning the INFLUX Project and the data collected, please visit https://influx.psu.edu.

4 Conclusions

The INFLUX EC network has become a vital component of the multivariate INFLUX data set. Micrometeorological methods like EC can bridge the gap between land surface modeling and atmospheric inverse methods used to quantify urban GHG fluxes. The INFLUX EC flux data expands the growing

https://doi.org/10.5194/essd-2025-232
Preprint. Discussion started: 16 June 2025

database of urban flux measurements. Data representative of the range of land-atmosphere fluxes encountered in this region was obtained by deploying multiple sites representative of the land cover of the city and its surroundings. We hope the data availability will support cross-collaboration between projects involving urban environments.

Author contributions. NM, SR, and KD conceived and coordinated the INFLUX project. KD conceptualized the EC flux measurement strategies for INFLUX. SR and NM installed the instrumentation, and SR, NM, and BA worked on maintaining the currently deployed instruments. BJH oversaw the data acquisition and monitoring system, and BJH and JH worked to create the system. BA, HK, SM, and JH oversee data processing and quality control. JH led the writing of this document, and all authors assisted in editing and reviewing this document. SM and JH helped create footprint climatologies for mixed urban towers.

Competing interests. The authors declare that they have no conflict of interest.

Acknowledgements.
We thank Brady Hardiman for assistance locating the sites for US-INa and US-INb and the Crown Hill Cemetery and The Fort Golf Resort for access to these sites. We thank Hal Truax, Dave Rhoads, and Andy Mohr for allowing us to deploy flux towers on their property. We also thank (folks who let us on INc, INg, and INd – get info from Scott and Tasha). We thank Daniel Sarmiento for leading the instrumentation and data acquisition from US-INf's EC flux measurements.

Financial support.

This work was supported by the US National Institute of Standards and Technology's urban GHG testbeds program, award numbers 70NANB10H245, 70NANB23H188, 70NANB19H128, and 70NANB15H336. HK was partly supported by Penn State's Institute of Energy and the Environment.

References

Aubinet, M., Vesala Timo, and Papale, D.: Eddy Covariance, edited by: Aubinet, M., Vesala, T., and Papale, D., Springer Netherlands, Dordrecht, 0–438 pp., 2012.

Baldocchi, D., Falge, E., Gu, L., Olson, R., Hollinger, D., Running, S., Anthoni, P., Bernhofer, C., Davis, K., Evans, R., Fuentes, J., Goldstein, A., Katul, G., Law, B., Lee, X., Malhi, Y., Meyers, T., Munger, W., Oechel, W., Paw, K. T., Pilegaard, K., Schmid, H. P., Valentini, R., Verma, S., Vesala, T., Wilson, K., and Wofsy, S.: FLUXNET: A New Tool to Study the Temporal and Spatial Variability of Ecosystem–Scale Carbon Dioxide, Water Vapor, and Energy Flux Densities, Bull Am Meteorol Soc, 82, 2415–2434, https://doi.org/10.1175/1520-0477(2001)082<2415:FANTTS>2.3.CO;2, 2001.

Biraud, S., Chen, J., Christen, A., Davis, K., Lin, J., McFadden, J., Miller, C., Nemitz, E., Schade, G., Stagakis, S., Turnbull, J., and Vogt, T.: Eddy Covariance Measurements in Urban Environments: White paper prepared by the AmeriFlux Urban Fluxes ad hoc committee, 2021.

https://doi.org/10.5194/essd-2025-232
Preprint. Discussion started: 16 June 2025

Open Access Earth System Science Data Discussions

Burba, G.: Eddy Covariance Method for Scientific, Industrial, Agricultural, and Regulatory Applications; a field book on measuring ecosystem gas exchange and areal emission rates, LI-COR Biosciences, Lincoln, Nebraska, xii–331 pp., 2013.

Crawford, B. and Christen, A.: Spatial source attribution of measured urban eddy covariance CO2 fluxes, Theor Appl Climatol, 119, 733–755, https://doi.org/10.1007/s00704-014-1124-0, 2015.

Davis, K. J., Deng, A., Lauvaux, T., Miles, N. L., Richardson, S. J., Sarmiento, D. P., Gurney, K. R., Hardesty, R. M., Bonin, T. A., Brewer, W. A., Lamb, B. K., Shepson, P. B., Harvey, R. M., Cambaliza, M. O., Sweeney, C., Turnbull, J. C., Whetstone, J., and Karion, A.: The Indianapolis Flux Experiment (INFLUX): A test-bed for developing urban greenhouse gas emission measurements, Elementa: Science of the Anthropocene, 5, https://doi.org/10.1525/elementa.188, 2017.

Davis K. J. AmeriFlux BASE US-INa INFLUX - Cemetery Turfgrass Tower, Ver. 1-5, AmeriFlux AMP, (data set), https://doi.org/10.17190/AMF/2001300, 2023a.

Davis K. J. AmeriFlux BASE US-INb INFLUX - Golf Course, Ver. 1-5, AmeriFlux AMP, (data set), https://doi.org/10.17190/AMF/2001301, 2023b.

Davis K. J. AmeriFlux BASE US-INc INFLUX - Downtown Indianapolis (Site-3), Ver. 1-5, AmeriFlux AMP, (data set), https://doi.org/10.17190/AMF/1987603, 2023c.

Davis K. J. AmeriFlux BASE US-INd INFLUX - Agricultural Site East near Pittsboro, Ver. 1-5, AmeriFlux AMP, (data set), https://doi.org/10.17190/AMF/2001302, 2023d.

Davis K. J. AmeriFlux BASE US-INe INFLUX - Agricultural Site West near Pittsboro, Ver. 1-5, AmeriFlux AMP, (data set), https://doi.org/10.17190/AMF/2001303, 2023e.

Davis K. J. AmeriFlux BASE US-INf INFLUX - East 21st St (Site 2), Ver. 1-5, AmeriFlux AMP, (data set), https://doi.org/10.17190/AMF/2001304, 2023f.

Davis K. J. AmeriFlux BASE US-INg INFLUX - Wayne Twp Comm (Site-7), Ver. 1-5, AmeriFlux AMP, (data set), https://doi.org/10.17190/AMF/2001305, 2023g.

Davis K. J. AmeriFlux BASE US-INi INFLUX - Agricultural Site East of Indianapolis (Site-9a), Ver. 1-5, AmeriFlux AMP, (data set), https://doi.org/10.17190/AMF/2001306, 2023h.

Davis K. J. AmeriFlux BASE US-INj INFLUX - Agricultural Site East of Indianapolis (Site-9b), Ver. 1-5, AmeriFlux AMP, (data set), https://doi.org/10.17190/AMF/2001307, 2023i.

Davis K. J. AmeriFlux BASE US-INn INFLUX - Agricultural Site West of Indianapolis (Site-14a), Ver. 1-5, AmeriFlux AMP, (data set), https://doi.org/10.17190/AMF/2001308, 2023j.

Davis K. J. AmeriFlux BASE US-INn INFLUX - Agricultural Site West of Indianapolis (Site-14b), Ver. 1-5, AmeriFlux AMP, (data set), https://doi.org/10.17190/AMF/2001309, 2023k.

https://doi.org/10.5194/essd-2025-232
Preprint. Discussion started: 16 June 2025

Deng, A., Lauvaux, T., Miles, N. L., Davis, K. J., Barkley, Z. R. Meteorological fields over Indianapolis, IN from the Weather Research and Forecasting model (WRF v3.5.1), Penn State DataCommons [data set], https://doi.org/10.26208/z04g-3h91, 2020.

Dragoni, D., Schmid, H. P., Wayson, C., Potters, H., Grimmond, S., and Randolph, J.: Evidence of increased net ecosystem productivity associated with a longer vegetated season in a deciduous forest in south-central Indiana, USA, Glob Chang Biol, 17, 886–897, https://doi.org/10.1111/j.1365-2486.2010.02281.x, 2011.

Foken, T.: Micrometeorology, Carmen J. Nappo., Springer, 2008.

Foken, Th. and Wichura, B.: Tools for quality assessment of surface-based flux measurements, Agric For Meteorol, 78, 83–105, https://doi.org/10.1016/0168-1923(95)02248-1, 1996.

Gurney, K. R., Patarasuk R., Liang, J., Yuyu, Z., O'Keeffe, D., Hutchins, M., Huang, J., Song, Y., Rao, P., Wong, T. M., Whetstone, J. R., Hestia Fossil Fuel Carbon Dioxide Emissions for Indianapolis, Indiana, National Institute of Standards and Technology, NIST Public Data Repository [data set], https://doi.org/10.18434/T4/1503341, 2018.

Horne, J. P., Davis, K. J. Vegetation Photosynthesis and Respiration Model (VPRM) run for 2019 over Indianapolis, IN, using a turfgrass PFT, Penn State DataCommons [data set], https://doi.org/10.26208/zs32-5n02, 2024.

Horne, J. P., Jin, C., Miles, N. L., Richardson, S. J., Murphy, S. L., Wu, K., and Davis, K. J.: The Impact of Turfgrass on Urban Carbon Dioxide Fluxes in Indianapolis, Indiana, USA, https://doi.org/10.1029/2024JG008477, 2025.

Järvi, L., Rannik, U., Kokkonen, T. V., Kurppa, M., Karppinen, A., Kouznetsov, R. D., Rantala, P., Vesala, T., and Wood, C. R.: Uncertainty of eddy covariance flux measurements over an urban area based on two towers, Atmos Meas Tech, 11, 5421–5438, https://doi.org/10.5194/amt-11-5421-2018, 2018.

Kaimal, J. C., Wyngaard, J. C., Izumi, Y., and Coté, O. R.: Spectral characteristics of surface-layer turbulence, Quarterly Journal of the Royal Meteorological Society, 98, 563–589, https://doi.org/10.1002/qj.49709841707, 1972.

Karion, A., Ghosh, S., Lopez-Coto, I., Mueller, K., Gourdji, S., Pitt, J., and Whetstone, J.: Methane Emissions Show Recent Decline but Strong Seasonality in Two US Northeastern Cities, Environ Sci Technol, 57, 19565–19574, https://doi.org/10.1021/acs.est.3c05050, 2023.

Kent, C. W., Lee, K., Ward, H. C., Hong, J. W., Hong, J., Gatey, D., and Grimmond, S.: Aerodynamic roughness variation with vegetation: analysis in a suburban neighbourhood and a city park, Urban Ecosyst, 21, 227–243, https://doi.org/10.1007/s11252-017-0710-1, 2018.

Kljun, N., Calanca, P., Rotach, M. W., and Schmid, H. P.: A simple two-dimensional parameterisation for Flux Footprint Prediction (FFP), Geosci Model Dev, 8, 3695–3713, https://doi.org/10.5194/gmd-8-3695-2015, 2015.

https://doi.org/10.5194/essd-2025-232
Preprint. Discussion started: 16 June 2025

Kotthaus, S. and Grimmond, C. S. B.: Energy exchange in a dense urban environment – Part I: Temporal variability of long-term observations in central London, Urban Clim, 10, 261–280, https://doi.org/10.1016/j.uclim.2013.10.002, 2014.

Lan, C., Mauder, M., Stagakis, S., Loubet, B., D'Onofrio, C., Metzger, S., Durden, D., and Herig-Coimbra, P.-H.: Intercomparison of eddy-covariance software for urban tall-tower sites, Atmos Meas Tech, 17, 2649–2669, https://doi.org/10.5194/amt-17-2649-2024, 2024.

Lauvaux, T., Gurney, K. R., Miles, N. L., Davis, K. J., Richardson, S. J., Deng, A., Nathan, B. J., Oda, T., Wang, J. A., Hutyra, L., and Turnbull, J.: Policy-relevant assessment of urban CO2 emissions, Environ Sci Technol, 54, 10237–10245, https://doi.org/10.1021/acs.est.0c00343, 2020.

Lee, X. and Massman, W. J.: A Perspective on Thirty Years of the Webb, Pearman and Leuning Density Corrections, Boundary Layer Meteorol, 139, 37–59, https://doi.org/10.1007/s10546-010-9575-z, 2011.

Lee, X., Massman, W., and Law, B.: Handbook of Micrometeorology, edited by: Lee, X., Massman, W., and Law, B., Springer Netherlands, Dordrecht, 1–250 pp., https://doi.org/10.1007/1-4020-2265-4, 2004.

Lipson, M., Grimmond, S., Best, M., Chow, W. T. L., Christen, A., Chrysoulakis, N., Coutts, A., Crawford, B., Earl, S., Evans, J., Fortuniak, K., Heusinkveld, B. G., Hong, J.-W., Hong, J., Järvi, L., Jo, S., Kim, Y.-H., Kotthaus, S., Lee, K., Masson, V., McFadden, J. P., Michels, O., Pawlak, W., Roth, M., Sugawara, H., Tapper, N., Velasco, E., and Ward, H. C.: Harmonized gap-filled datasets from 20 urban flux tower sites, Earth Syst Sci Data, 14, 5157–5178, https://doi.org/10.5194/essd-14-5157-2022, 2022.

Liu, H. Z., Feng, J. W., Järvi, L., and Vesala, T.: Four-year (2006-2009) eddy covariance measurements of CO 2 flux over an urban area in Beijing, Atmos Chem Phys, 12, 7881–7892, https://doi.org/10.5194/acp-12-7881-2012, 2012.

Lwasa, S., K.C. Seto, X. Bai, H. Blanco, K.R. Gurney, Ş. Kılkış, O. Lucon, J. Murakami, J. Pan, A. Sharifi, and Y. Yamagata: Urban Systems and Other Settlements, in: Climate Change 2022 - Mitigation of Climate Change, Cambridge University Press, 861–952, https://doi.org/10.1017/9781009157926.010, 2023.

Mauder, M. and Foken, T.: Documentation and Instruction Manual of the Eddy Covariance Software Package TK2, 1 pp., 2004.

Menzer, O. and McFadden, J. P.: Statistical partitioning of a three-year time series of direct urban net CO2 flux measurements into biogenic and anthropogenic components, Atmos Environ, 170, 319–333, https://doi.org/10.1016/j.atmosenv.2017.09.049, 2017.

Miles, N. L., Richardson, S. J., Lauvaux, T., Davis, K. J., Balashov, N. V., Deng, A., Turnbull, J. C., Sweeney, C., Gurney, K. R., Patarasuk, R., Razlivanov, I., Cambaliza, M. O. L., and Shepson, P. B.: Quantification of urban atmospheric boundary layer greenhouse gas dry mole fraction enhancements in the dormant season: Results from the Indianapolis Flux Experiment (INFLUX), Elementa: Science of the Anthropocene, 5, https://doi.org/10.1525/elementa.127, 2017a.

https://doi.org/10.5194/essd-2025-232
Preprint. Discussion started: 16 June 2025

Miles, N. L., Richardson, S. J., Davis, K. J., Haupt, B. J.: In-situ tower atmospheric measurements of carbon dioxide, methane and carbon monoxide mole fraction for the Indianapolis Flux (INFLUX) project, Indianapolis, IN, USA., Penn State DataCommons [data set], https://doi.org/10.18113/D37G6P, 2017b.

Milesi, C., Running, S. W., Elvidge, C. D., Dietz, J. B., Tuttle, B. T., and Nemani, R. R.: Mapping and Modeling the Biogeochemical Cycling of Turf Grasses in the United States, Environ Manage, 36, 426–438, https://doi.org/10.1007/s00267-004-0316-2, 2005.

Moncrieff, J. B., Massheder, J. M., de Bruin, H., Elbers, J., Friborg, T., Heusinkveld, B., Kabat, P., Scott, S., Soegaard, H., and Verhoef, A.: A system to measure surface fluxes of momentum, sensible heat, water vapour and carbon dioxide, J Hydrol (Amst), 188–189, 589–611, https://doi.org/10.1016/S0022-1694(96)03194-0, 1997.

Moore, C. J.: Frequency response corrections for eddy correlation systems, Boundary Layer Meteorol, 37, 17–35, https://doi.org/10.1007/BF00122754, 1986.

Murphy, S. L., Davis, K. J., Miles, N. L. Penn State Department of Meteorology Vegetation Photosynthesis and Respiration Model (VPRM) runs for Indianapolis, IN, from 2012 through 2021, Penn State DataCommons [data set], https://doi.org/10.26208/zs32-5n02, 2024.

Ng, B. J. L., Hutyra, L. R., Nguyen, H., Cobb, A. R., Kai, F. M., Harvey, C., and Gandois, L.: Carbon fluxes from an urban tropical grassland, Environmental Pollution, 203, 227–234, https://doi.org/10.1016/j.envpol.2014.06.009, 2015.

Nicolini, G., Antoniella, G., Carotenuto, F., Christen, A., Ciais, P., Feigenwinter, C., Gioli, B., Stagakis, S., Velasco, E., Vogt, R., Ward, H. C., Barlow, J., Chrysoulakis, N., Duce, P., Graus, M., Helfter, C., Heusinkveld, B., Järvi, L., Karl, T., Marras, S., Masson, V., Matthews, B., Meier, F., Nemitz, E., Sabbatini, S., Scherer, D., Schume, H., Sirca, C., Steeneveld, G.-J., Vagnoli, C., Wang, Y., Zaldei, A., Zheng, B., and Papale, D.: Direct observations of CO2 emission reductions due to COVID-19 lockdown across European urban districts, Science of The Total Environment, 830, 154662, https://doi.org/10.1016/j.scitotenv.2022.154662, 2022.

Pahari, R., Leclerc, M. Y., Zhang, G., Nahrawi, H., and Raymer, P.: Carbon dynamics of a warm season turfgrass using the eddy-covariance technique, Agric Ecosyst Environ, 251, 11–25, https://doi.org/10.1016/j.agee.2017.09.015, 2018.

Papale, D., Antoniella, G., Nicolini, G., Gioli, B., Zaldei, A., Vogt, R., Feigenwinter, C., Stagakis, S., Chrysoulakis, N., Järvi, L., Nemitz, E., Helfter, C., Barlow, J., Meier, F., Velasco, E., Christen, A., and Masson, V.: Clear evidence of reduction in urban CO 2 emissions as a result of COVID-19 lockdown across Europe, 2020.

Papale, D., Andreas, C., Davis, K., Christian, F., Beniamino Gioli, Leena, J., Bradley, M., Erik, V., and Roland, V.: Eddy covariance flux observations., GAW Report, 275, 114–123, 2022.

Pastorello, G., Trotta, C., Canfora, E., Chu, H., Christianson, D., Cheah, Y. W., Poindexter, C., Chen, J., Elbashandy, A., Humphrey, M., Isaac, P., Polidori, D., Ribeca, A., van Ingen, C., Zhang, L., Amiro, B.,

https://doi.org/10.5194/essd-2025-232
Preprint. Discussion started: 16 June 2025

Ammann, C., Arain, M. A., Ardö, J., Arkebauer, T., Arndt, S. K., Arriga, N., Aubinet, M., Aurela, M., Baldocchi, D., Barr, A., Beamesderfer, E., Marchesini, L. B., Bergeron, O., Beringer, J., Bernhofer, C., Berveiller, D., Billesbach, D., Black, T. A., Blanken, P. D., Bohrer, G., Boike, J., Bolstad, P. V., Bonal, D., Bonnefond, J. M., Bowling, D. R., Bracho, R., Brodeur, J., Brümmer, C., Buchmann, N., Burban, B., Burns, S. P., Buysse, P., Cale, P., Cavagna, M., Cellier, P., Chen, S., Chini, I., Christensen, T. R., Cleverly, J., Collalti, A., Consalvo, C., Cook, B. D., Cook, D., Coursolle, C., Cremonese, E., Curtis, P. S., D'Andrea, E., da Rocha, H., Dai, X., Davis, K. J., De Cinti, B., de Grandcourt, A., De Ligne, A., De Oliveira, R. C., Delpierre, N., Desai, A. R., Di Bella, C. M., di Tommasi, P., Dolman, H., Domingo, F., Dong, G., Dore, S., Duce, P., Dufrêne, E., Dunn, A., Dušek, J., Eamus, D., Eichelmann, U., ElKhidir, H. A. M., Eugster, W., Ewenz, C. M., Ewers, B., Famulari, D., Fares, S., Feigenwinter, I., Feitz, A., Fensholt, R., Filippa, G., Fischer, M., Frank, J., Galvagno, M., Gharun, M., Gianelle, D., et al.: The FLUXNET2015 dataset and the ONEFlux processing pipeline for eddy covariance data, Sci Data, 7, 225, https://doi.org/10.1038/s41597-020-0534-3, 2020.

Paw U, K. T., Baldocchi, D. D., Meyers, T. P., and Wilson, K. B.: Correction Of Eddy-Covariance Measurements Incorporating Both Advective Effects And Density Fluxes, Boundary Layer Meteorol, 97, 487–511, https://doi.org/10.1023/A:1002786702909, 2000.

Pawlak, W. and Fortuniak, K.: Eddy covariance measurements of the net turbulent methane flux in the city centre-results of 2-year campaign in Lodz, Poland, Atmos Chem Phys, 16, 8281–8294, https://doi.org/10.5194/acp-16-8281-2016, 2016.

Pérez-Ruiz, E. R., Vivoni, E. R., and Templeton, N. P.: Urban land cover type determines the sensitivity of carbon dioxide fluxes to precipitation in Phoenix, Arizona, PLoS One, 15, https://doi.org/10.1371/journal.pone.0228537, 2020.

Peters, E. B. and McFadden, J. P.: Continuous measurements of net CO2 exchange by vegetation and soils in a suburban landscape, J Geophys Res Biogeosci, 117, https://doi.org/10.1029/2011JG001933, 2012.

Peters, E. B., Hiller, R. V., and McFadden, J. P.: Seasonal contributions of vegetation types to suburban evapotranspiration, J Geophys Res Biogeosci, 116, https://doi.org/10.1029/2010JG001463, 2011.

Richardson, S. J., Miles, N. L., Davis, K. J., Lauvaux, T., Martins, D. K., Turnbull, J. C., McKain, K., Sweeney, C., and Cambaliza, M. O. L.: Tower measurement network of in-situ CO2, CH4, and CO in support of the Indianapolis FLUX (INFLUX) Experiment, Elementa: Science of the Anthropocene, 5, https://doi.org/10.1525/elementa.140, 2017.

Richardson, S. J., Miles, N. L., Haupt, B. J., Ahlswede, B., Horne, J. P., Davis, K. J. Eddy Covariance High-Frequency Data for Turfgrass and Pasture in Indianapolis, Indiana and Montgomery County, Maryland (US-INa, US-INb, US-BWa, US-BWb, US-BWc), Penn State DataCommons [data set], https://doi.org/10.26208/CJTC-KS26, 2023a.

Richardson, S. J., Miles, N. L., Haupt, B. J., Ahlswede, B., Horne, J. P., Davis, K. J. Eddy Covariance High-Frequency Data for Agricultural Sites near Indianapolis, Indiana (US-INd, US-INe, US-INi, US-INj, US-INn, US-INp), Penn State DataCommons [data set], https://doi.org/10.26208/fsy8-h855, 2023b.

Richardson, S. J., Miles, N. L., Haupt, B. J., Ahlswede, B., Horne, J. P., Davis, K. J. Eddy Covariance High-Frequency Data for Urban and Suburban Sites in Indianapolis, Indiana (US-INc, US-INg), Penn State DataCommons [data set], https://doi.org/10.26208/2NT2-RS82, 2023c.

Sarmiento, D. P., Davis, K. J. Eddy covariance flux tower data for Indianapolis, IN (INFLUX project), Penn State DataCommons [data set], https://doi.org/10.17190/AMF/2001304, 2017.

Schmid, H. P., Grimmond, S., Cropley, F., Offerle, B., and Su, H.-B.: Measurements of CO_2 and energy fluxes over a mixed hardwood forest in the mid-western United States, Agric For Meteorol, 103, 357–374, https://doi.org/10.1016/S0168-1923(00)00140-4, 2000.

Semerjian, H. G. and Whetstone, J. R.: Urban greenhouse gas measurements :, https://doi.org/10.6028/NIST.TN.2145, 2021.

Stewart, I. D. and Oke, T. R.: Local climate zones for urban temperature studies, Bull Am Meteorol Soc, 93, 1879–1900, https://doi.org/10.1175/BAMS-D-11-00019.1, 2012.

U.S. Department of Agriculture, Natural Resource Conservation Service (NRCS), Indiana State Office, and the Indiana Geographic Information Council (IGIC), under separate BAA Agreements in partnership with the United States Geological Services (USGS) 3DEP Program. Indiana 3DEP Lidar Base Products. (data set), https://igic.memberclicks.net/indiana-s-new-3dep-lidar-data-and-informational-resources, 2021.

Vickers, D. and Mahrt, L.: Quality Control and Flux Sampling Problems for Tower and Aircraft Data, J Atmos Ocean Technol, 14, 512–526, https://doi.org/10.1175/1520-0426(1997)014<0512:QCAFSP>2.0.CO;2, 1997.

Vogel, E., Davis, K. J., Wu, K., Miles, N. L., Richardson, S. J., Gurney, K. R., Monteiro, V., Roest, G. S., Kenion, H. C. R., and Horne, J. P.: Using eddy-covariance to measure the effects of COVID-19 restrictions on CO_2 emissions in a neighborhood of Indianapolis, IN, Carbon Manag, 15, https://doi.org/10.1080/17583004.2024.2365900, 2024.

Vogt, R., Christen, A., Rotach, M. W., Roth, M., and Satyanarayana, A. N. V.: Temporal dynamics of CO_2 fluxes and profiles over a Central European city, Theor Appl Climatol, 84, 117–126, https://doi.org/10.1007/s00704-005-0149-9, 2006.

Webb, E. K., Pearman, G. I., and Leuning, R.: Correction of flux measurements for density effects due to heat and water vapour transfer, Quarterly Journal of the Royal Meteorological Society, 106, 85–100, https://doi.org/10.1002/qj.49710644707, 1980.

Wilczak, J. M., Oncley, S. P., and Stage, S. A.: Sonic Anemometer Tilt Correction Algorithms, Boundary Layer Meteorol, 99, 127–150, https://doi.org/10.1023/A:1018966204465, 2001.

Wu, K., Davis, K. J., Miles, N. L., Richardson, S. J., Lauvaux, T., Sarmiento, D. P., Balashov, N. V., Keller, K., Turnbull, J., Gurney, K. R., Liang, J., and Roest, G.: Source decomposition of eddy-covariance

https://doi.org/10.5194/essd-2025-232
Preprint. Discussion started: 16 June 2025

CO_2 flux measurements for evaluating a high-resolution urban CO_2 emissions inventory, Environmental Research Letters, 17, https://doi.org/10.1088/1748-9326/ac7c29, 2022.

Yadav, V., Verhulst, K., Duren, R., Thorpe, A., Kim, J., Keeling, R., Weiss, R., Cusworth, D., Mountain, M., Miller, C., and Whetstone, J.: A declining trend of methane emissions in the Los Angeles basin from 2015 to 2020, Environmental Research Letters, 18, 034004, https://doi.org/10.1088/1748-9326/acb6a9, 2023.

Yi, C., Davis, K. J., Bakwin, P. S., Berger, B. W., and Marr, L. C.: Influence of advection on measurements of the net ecosystem-atmosphere exchange of CO_2 from a very tall tower, Journal of Geophysical Research: Atmospheres, 105, 9991–9999, https://doi.org/10.1029/2000JD900080, 2000.